J. Water Environ. Nanotechnol., 4(1): 17-30 Winter 2019

ORIGINAL RESEARCH PAPER

Investigation and Comparison of Cobalt ferrite composite nanoparticles with individual Iron oxide and Cobalt oxide nanoparticles in azo dyes removal

Janan Parhizkar*, Mohammad Hossein Habibi

Nanotechnology Laboratory, Department of Chemistry, University of Isfahan, Isfahan, Iran

Received: 2018-11-21 Accepted: 2018-12-25 Published: 2019-02-01

ABSTRACT

Photocatalytic treatment of wastewater from azo dyes with semiconductors promises efficient method to refine water. Cobalt ferrite is synthesized and utilized for dye removal as a semiconducting composite. To compare the photocatalytic performance of its individual oxides, Co_3O_4 and FeO were synthesized by the same route and applied to water treatment. In this work, cobalt ferrite, Co_3O_4 and FeO nanoparticles were synthesized as photocatalysts by employing wet chemical method with chloride precursors respectively ($CoCl_2.6H_2O$ & $FeCl_3.6H_2O$, $CoCl_2.6H_2O$, $FeCl_3$. $6H_2O$). The synthesized photocatalysts were characterized by powder X-ray diffraction (XRD), Fourier transforms infrared spectroscopy (FTIR), diffuse reflectance spectroscopy (DRS) and field emission scanning electron microscopy (FESEM). The obtained photocatalysts were coated on the glass by Dr. Blade method. The degradation of Acid Black 1 (AB1) and Reactive Red 4 (RR4) by cobalt ferrite, Co_3O_4 and FeO were carried out under UV light irradiation to investigate their photocatalytic activities. FeO nanoparticles were found as the best photocatalyst to achieve maximum degradation of Azo dyes. The high degradation performance of FeO can be attributed to the photo-Fenton phenomena-like furthermore photocatalytic process. The Degradation rate of AB1 by photocatalysts decreases in the order of FeO > Co_3O_4> $CoFe_2O_4$. The photocatalytic degradation kinetics of AB1 using photocatalyst nanoparticles was found to be the first order kinetic rate. For RR4, $CoFe_2O_4$ followed first order, FeO and Co_3O_4 followed a second order kinetic rate. Presence of iron oxide in cobalt ferrite improved the photocatalytic performance..

Keywords: *Azo dye; Kinetic; Nanoparticle; Photocatalytic degradation; Photo-Fenton phenomena*

How to cite this article

Parhizkar J, Habibi MH. Investigation and Comparison of Cobalt ferrite composite nanoparticles with individual Iron oxide and Cobalt oxide nanoparticles in azo dyes removal. J. Water Environ. Nanotechnol., 2019; 4(1): 17-30.

DOI: 10.22090/jwent.2019.01.002

INTRODUCTION

One of the main groups of organic compounds is azo materials. These components have the most application in azo dye synthesis that involves an extensive spectrum of colors. Azo dyes are widely used in textile industries. The azo functional group(–N=N–) in azo dyes is a carcinogen, toxic and bio recalcitrant [1-2]. Textile wastewater is infected with azo dyes even after conventional treatment. Various chemical and physical treatment techniques and processes have been used to remove dye pollutants from contaminated water. The adsorption [3-5] and advanced oxidation processes [6-7] are successful methods for dye removal. The advanced oxidation process is based on the in situ production of highly reactive hydroxyl radicals (·OH) that react with azo dyes and degrade them. Photo-Fenton process is an example of an advanced oxidation process. Photocatalysis uses a semiconductor under illumination light (ultraviolet or visible) to generate electron/hole pairs with the ability to degrade azo dyes. Li et al.[**8**] reported alumina supported hematite with high activity and stability. They evaluated the catalyst activity with orange II. Fe_2O_3/ Alumina showed higher activity than Fe_2O_3/ silica and bare hematite because of

* Corresponding Author Email: *jananparhizkar@gmail.com*

reduced particle size of hematite and the enhanced surface adsorption of dye on the catalyst.

Marcio Rodriques and his coworkers [9] have synthesized zero valent iron nanoparticles in variable synthesis conditions and used them in the degradation of the azo dye disperse red 1. Nano zero valent iron particles yielded high color removal in a short time (around 98% in 10 min).

Magnetite is another compound of iron which was used in the degradation of dye pollutants [10-12].

Cobalt oxides such as CoO or Co_3O_4 are p-type semiconductors with interesting electronic and magnetic properties. They have found applications as an efficient catalyst[13], high temperature solar selective absorber[14], pigment for glasses and ceramics[15] etc. Cai and his coworkers [16] synthesized Co_3O_4 / $BiVO_4$ composite by the impregnation method. The photocatalyst has exhibited enhanced photocatalytic activity for phenol degradation. CO_3O_4 nanoparticles were used as photocatalyst for degradation of methyl orange, Diclofenac Sodium [17], Cr(VI) and dye removal[18].

Nanosize spinel ferrite particles recently have received considerable attention because of their wide applications. $CoFe_2O_4$, one of the most significant spinel ferrite exhibited remarkable photocatalytic properties [19].

Meso-macroporous nanospheres of $CoFe_2O_4$ were applied as adsorbent and photocatalyst for Cr(VI) removal and anionic dye degradation (Methyl Orange), respectively [20].

$CoFe_2O_4$ nanoparticles assembled on mesoporous graphitic carbon nitride were tested in the photocatalytic degradation of Malachite Green and 93% degradation efficiency was obtained [21]. The superparamagnetic cobalt ferrite nanoparticles offered heterogeneous and recoverable catalyst. The Catalyst separation from reaction media and recycling it are of practical problems. To overcome the problem of catalyst separation and making recyclable photocatalyst, coating of nanoparticles on the inert substrate can be an appropriate option. In this project, photocatalyst nanoparticles were stabilized on the glass by doctor bade technique.

Although, a lot of researches have been devoted to investigating the photocatalytic performance of cobalt ferrite, Iron oxides, and cobalt oxides nanoparticles, there are rare articles about the comparison of $CoFe_2O_4$ with its single metals oxide [19]. This comparison allows choosing the most suitable option for achieving more efficient water purification in the shortest possible time.

In this work, the aim is a comparison between the performance of $CoFe_2O_4$ as a composite with Co_3O_4 and FeO as (single oxides) individual oxides in photocatalytic degradation of azo dyes. $CoFe_2O_4$, FeO and Co_3O_4 nanoparticles were synthesized by the same route (wet chemical method). The structural, optical and morphological properties of particles were investigated by XRD, FT-IR, DRS and FESEM analysis. The dye degradation performance of $CoFe_2O_4$, FeO and Co_3O_4 were evaluated by photodegradation of Reactive Red 4 and Acid Black 1. The kinetics of dye degradation by particles were investigated.

EXPERIMENTAL

Materials

The precursor materials, cobalt (II) chloride hexahydrate ($CoCl_2.6H_2O$) and iron (III) chloride hexahydrate ($FeCl_3.6H_2O$) were obtained from Merck Chemical Company. Sodium hydroxide (NaOH), Oleic acid ($C_{18}H_{34}O_2$), Acetic Acid ($C_2H_4O_2$), Terpineol ($C_{10}H_{18}O$), ethyl cellulose, Acid Black 1 ($C_{22}H_{14}N_6Na_2O_9S_2$) and Reactive Red 4 ($C_{32}H_{19}ClN_8O_{14}S_4Na_4$) were purchased from Sigma-Aldrich Chemical Co. Distilled water was used throughout.

Synthesis of Co_3O_4, FeO and $CoFe_2O_4$ nanoparticles by wet chemical route

To synthesize $CoFe_2O_4$ nanoparticles, as mentioned in our previous paper [22] Cobalt (II) chloride hexahydrate (5 mmol), 1.22 g and iron (III) chloride hexahydrate (10 mmol), 2.72 g were separately dissolved in double distilled water (25 mL) and placed in an ultrasonicator for 2 min. Two solutions were mixed and sodium hydroxide (25 mL, 3 M) was added and stirred up to pH = 12. Oleic acid as a chelating agent (1 mL) was added to the above suspension. The temperature of the suspension was raised to 80 °C with continued stirring for 1 h. The product was cooled to room temperature and the precipitate was separated by centrifuge, washed twice with double distilled water and ethanol. The precipitate was dried at 75 °C (dark brown powder), annealed at 600 °C for 10 h and black powder was obtained. The same experimental procedure as $CoFe_2O_4$ nanoparticles preparation was performed except adding cobalt(II) chloride hexahydrate solution and iron(III) chloride hexahydrate solution for preparing FeO and Co_3O_4 nanoparticles, respectively. Fig. 1 shows a Flow chart for wet chemical route preparation

of $CoFe_2O_4$ nanocomposite, Co_3O_4, and FeO nanoparticles.

Coating on glass using nanoparticles pastes by Doctor Blade method

A 0.8 g of each nano-powders prepared by wet chemical route was grinded by adding 130 µL of acetic acid and stirred for 5 min. 130 µL double distilled water was added and the solution was stirred for 1 min and this process repeated 5 times. Then 130 µL Ethanol was added and the solution was stirred for 1 min, and this process repeated 15 times, too. After this 15 ml ethanol, 3 mL terpineol and 0.4 g ethyl cellulose were added to 5 mL ethanol and the paste solution was sonicated for 1 min. The solvent was evaporated by stirring in the air and nanopowder/ ethyl cellulose terpineol paste was used for coating on the glass by Doctor Blade for $CoFe_2O_4$, $Co_3O_4$and FeO nanoparticles separately. The photocatalyst-coated glass was air dried, and sintered at 300 °C in the air to improve the contact between the film and the substrate. Fig. 2 shows Glass slides coated with a paste of $CoFe_2O_4$, FeO and Co_3O_4 nanoparticles prepared by a wet chemical route using Dr. Blade method.

Characterization

FT-IR absorption spectra of samples were obtained using KBr disks on an FT-IR 6300. Powder X-ray diffraction analysis was performed on a D8 Advance, BRUKER diffractometer in the diffraction angle range 2θ=5-80° with Cu Kα radiation (1.5406

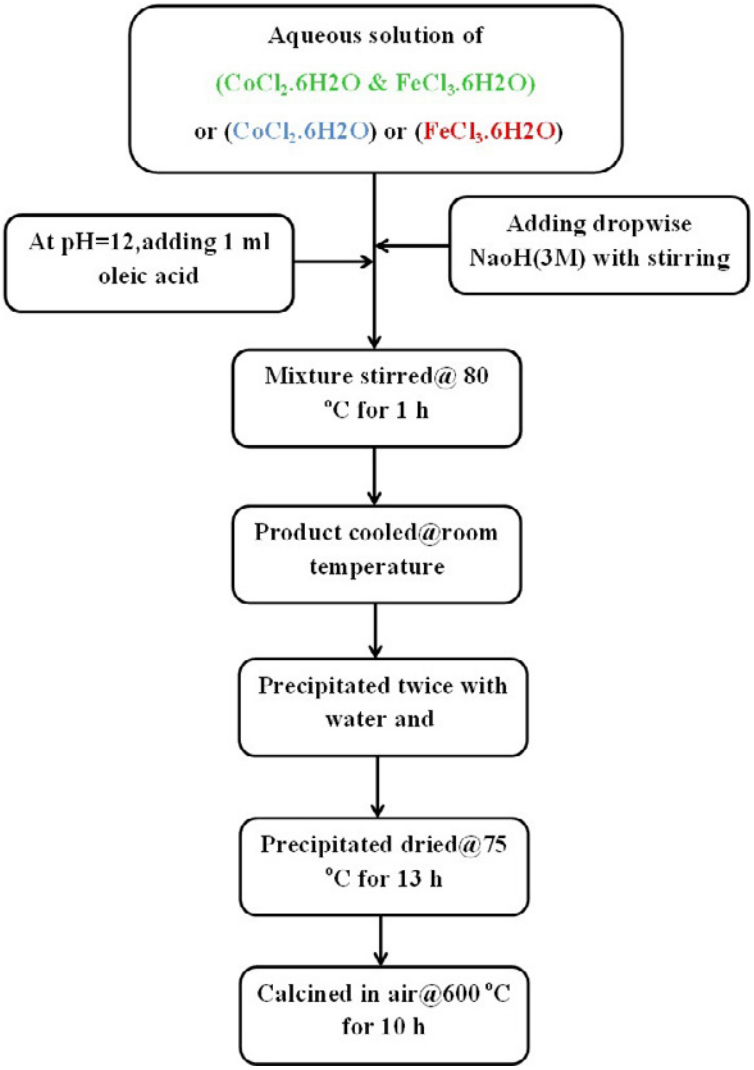

Fig. 1. Flow chart for wet chemical route preparation of cobalt ferrite nanocomposite, cobalt oxide and iron oxide nanoparticles.

A°). Diffuse reflectance spectra (DRS) were collected with a V-670, JASCO spectrophotometer and transformed to the absorption spectra according to the Tauc relationship. Field emission scanning electron microscopy (FESEM) images were taken on a Hitachi, S-4160 scanning electron microscope. The azo dyes solutions concentration was determined using its absorbance by a Cary 500 UV–Vis spectrophotometer.

Photocatalytic activity test

Photocatalytic degradation of Reactive Red 4 (RR4) and Acid Black 1 (AB1) in water was performed at room temperature exposed to UV light irradiation so as to evaluate the catalytic performance of photocatalysts. A 250 W Hg lamp was used as the light source. For all the degradation experiments, the photocatalyst coated on a glass slide was appointed in a Petri dish which contained 25 ml dye solution which exposed at O2 gas for 30 min. The area of the photocatalyst coated on glass was 11 cm2. The mixture of dye and photocatalyst coated on glass was stirred in the dark condition to allow mixture to establish sorption and desorption equilibrium of dye molecules by the photocatalyst nanoparticles. The light source was

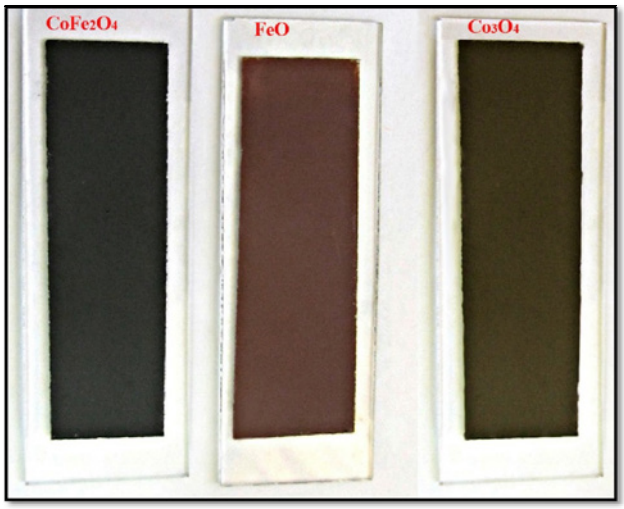

Fig. 2. Glass slides coated with paste of cobalt ferrite, Iron oxide and cobalt oxide nanoparticles prepared by wet chemical route using Dr Blade method.

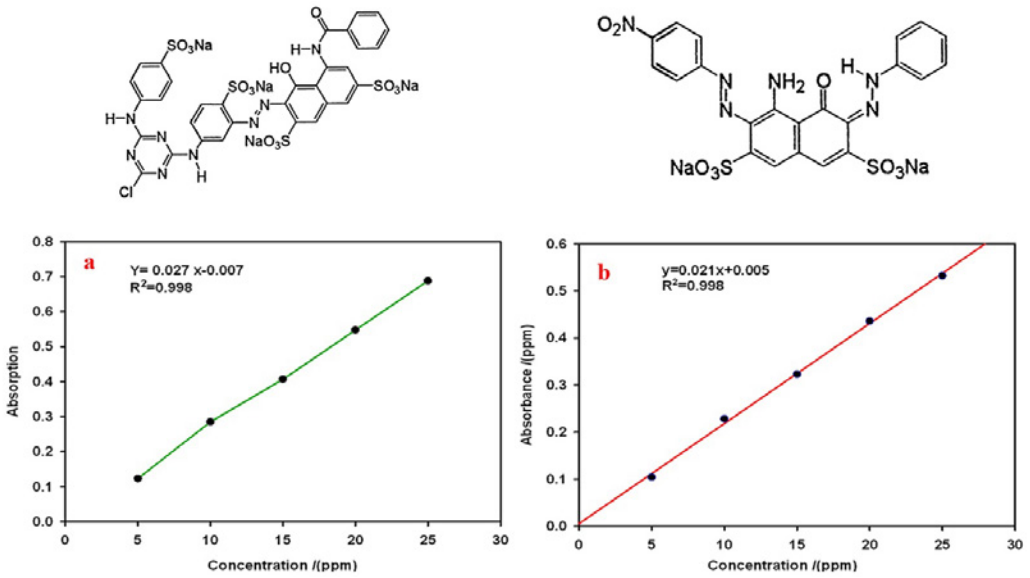

Fig. 3. The Concentration dependent spectra from different standard solutions and calibration curves: a) Reactive Red 4 and b) Acid Black 1.

placed about 20 cm away from the liquid surface of the mixture. To determine dye degradation percent by photocatalyst first standard solutions with different concentration of Reactive Red 4 and Acid Black 1were prepared and their UV-Vis spectra were recorded (inserted in Fig. 3) Then the graph of absorbance in maximum wavelength (λmax for AB1=616 & λmax= 534 for RR4) vs concentration was plotted and the equation of the most fitted line was obtained (Fig. 3). This equation was used to determine the concentration of dye by UV absorbance intensity of dye which degraded with the photocatalyst. The equation of calibration curves of Acid Black 1 and Reactive Red 4 has been inserted in Fig. 3. Then the mixture of dye and photocatalyst coated on glass was irradiated under a UV lamp to initiate photocatalytic degradation of azo dyes. During the reaction, at a determined interval time (15min) small amount of solution was analyzed by Cary 500 UV–Vis spectrophotometer. Relative degradation of each azo dye can be calculated as follows (Eq.1):

$$\text{Relative degradation (\%)} = (C0-Ct)/C0 \times 100 \quad (1)$$

Which Co and Ct were the dye concentrations at an initial time and after a Reaction period of t (min) under UV-light irradiation, respectively.

The photocatalytic degradation kinetics of azo dyes using photocatalysts nanoparticles coated on glass was appraised using the first order and second order equations given in the equations (Eq. 2) and (Eq. 3) and the plots were drawn and the first and second order constants were calculated.

$$ln\left(\frac{c_t}{c_0}\right) = k_{1app}\, t \quad (2)$$

$$\left(\frac{1}{c_t}\right) = \left(\frac{1}{c_0}\right) + k_2 t \quad (3)$$

Where C_0 is the initial concentration of azo dye solutions, C_t is the concentration of dye solutions at time t, k_{1app} is the first order constant, k_2, is the second order rate constant, t is the Ultra-Violet light exposure time. The regression correlation coefficient (R^2) of the first and second order plot was calculated. Then the equation with greater regression correlation coefficient was chosen as the kinetic order of dye degradation.

RESULT AND DISCUSSION

X-ray Diffraction Analysis

To characterize the crystalline structure of the samples, the XRD patterns of $CoFe_2O_4$, Co_3O_4 and FeO were obtained as shown in Fig. .4. All peaks from X-ray diffraction pattern of $CoFe_2O_4$ clearly matched well with face centered cubic (fcc) $CoFe_2O_4$ (JCPDS card 22-1086) [23-26], corresponding to Miller indices (111), (220), (311),

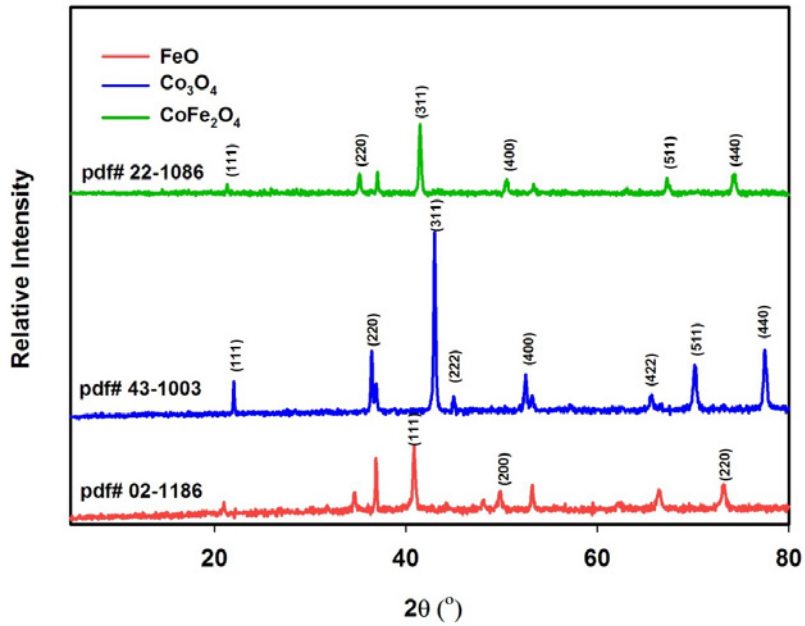

Fig. 4.XRD patterns of cobalt oxide, iron oxide, cobalt ferrite nanoparticles prepared by wet chemical route after calcination.

(400), (422), (511) and (440). The reflection from the XRD pattern displayed the spinel structure of $CoFe_2O_4$ with preferred orientation along (311) plane [27]. Unfortunately, the peak of impurity at 2θ = 36.93 was observed in the sample, which is related to NaCl crystals produced as a by-product during synthesis. For Co_3O_4, the diffraction peaks at 22.1, 36.4, 42.8, 44.8, 52.6, 65.6, 70.2 and 77.6 correspond to (111), (220), (311), (222), (400), (422), (511) and (440) planes of Co_3O_4 (JCPDS card no. 43.1003), respectively. For FeO, the diffraction peaks at 41.05, 49.8 and 73.17 correspond to (111), (200) and (220) planes of FeO (JCPDS card no.02.1186), respectively. Other peaks in the FeO diffraction pattern are related to sodium iron oxide ($NaFeO_2$) (JCPDS card no.20-1115) and halite (NaCl) (JCPDS card no.75-0306) presented in the sample. The average crystallite sizes of spinel $CoFe_2O_4$, FeO and Co_3O_4 were calculated from X-ray line broadening using Scherrer's equation and were found to be about 47 nm, 50 nm, and 40 nm, respectively.

FT-IR Spectroscopic Characterization

Fig. .5 shows the FTIR spectra of $CoFe_2O_4$, Co_3O_4, FeO nanoparticles annealed at 600 °C recorded between 3500 cm^{-1} and 400 cm^{-1}. The O–H stretching vibrations interacting through H bonds are observed at around 3430 cm^{-1} in three samples, 2927 cm^{-1} and the absorption band present at about 1623 and 1634 $cm^{-1}$is due to the bending of the absorbed water molecules [29]. The absorption band at 1113 cm_1 is the characteristic of $CoFe_2O_4$system and this may be due to the residual FeOOH. The absorption bands present at about 585 $cm^{-1}$and 410 cm^{-1} is due to the stretching vibrations of metal oxide in octahedral group complex Co(II) $-O^{2-}$ and Fe(III) $-O^{2-}$ tetrahedral group complex of the $CoFe_2O_4$ phase respectively which proves the existence of spinel ferrite [29- 30]. The peak at 666 cm^{-1} in FTIR spectrum of Co_3O_4 is attributed to Co–O vibrations where cobalt ions are in a tetrahedral position. The peak at 574 cm^{-1} is associated with Co–O vibration in the spinel lattice where cobalt cations are in octahedral positions. The band at 880 cm^{-1} is related to CoOOH or water of hydration [31-34]. In the FTIR spectrum of FeO, the peak observed at 1435 cm^{-1} is probably related to carbon dioxide vibrations adsorbed on the surface of nanoparticles. The strong absorption band at 570 and 484 cm^{-1} are evidence of Fe–O–Fe bonds.

UV-Vis diffuse reflectance Spectroscopic Characterization for optical properties

UV-Vis absorption spectroscopy was used to investigate the optical properties of $CoFe_2O_4$,

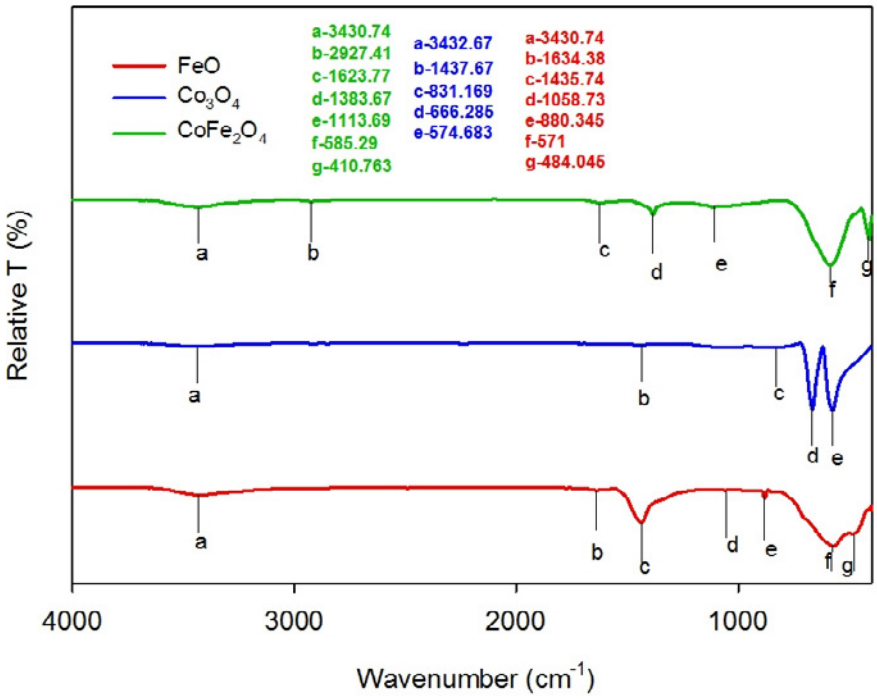

Fig. 5.FTIR spectra of cobalt oxide, iron oxide and cobalt ferrite nanoparticles prepared by wet chemical route after calcination

FeO and Co_3O_4 semiconducting nanoparticles. It should be noted that the optical properties of the nanoparticles mainly depend on the particle size. The band gap and surface roughness affect the absorbance of a semiconducting material [35-37]. Fig. 6 shows UV-Vis diffuse reflectance spectra and Tauk plots of $CoFe_2O_4$, FeO and Co_3O_4 nanoparticles. The peak at 332 nm in the absorption spectrum of $CoFe_2O_4$ is related to the transition of an electron from the valence band (VB) to the conduction band (CB) [38-40]. Co3O4 is a p-type semiconductor. There are two absorption peaks (λ=648 and 385nm) being obviously found in Fig. 6 for Co3O4 absorption spectrum which indicates ligand-metal charge transfer events O(II)→Co(III) and O(II) → Co(II), respectively [34]. Tauc plot is used to calculate the band gap of semiconducting materials [41]. The Tauc formula (Eq. (4)) depicting the relationship between the absorption coefficient and the incident photon is as follows:

$$\alpha h\nu = A(h\nu - Eg)^n \quad (4)$$

where α is the absorption coefficient, A is a constant and n is an index which assumes the values 1/2, 3/2, 2 and 3 depending on the nature of electronic transition, where n=1/2 for direct band gap semiconductors. An extrapolation of the linear region of the plot $(\alpha h\nu)2$ vs hv gives the value of the optical band gap Eg as shown in Fig.6. The measured band gap of $CoFe_2O_4$ was found to be 1.32 eV. For Co_3O_4, the band gap was measured in 2.17 eV. The energy band gap of FeO nanoparticle was 1.6 eV.

FESEM Analysis

Field emission scanning electron microscope (FESEM) was employed to investigate the morphology of samples (Fig. 7). It was found that the $CoFe_2O_4$ sample consisted of homogenous connected nanospheres (Fig. 7. c & f). $CoFe_2O_4$ nanoparticles had a diameter of about 48 nm. FESEM picture of Co_3O_4 shows that nanoparticles were separated and unsymmetrical octahedral (Fig. 7. b and e) and the size of particles was about 73nm.

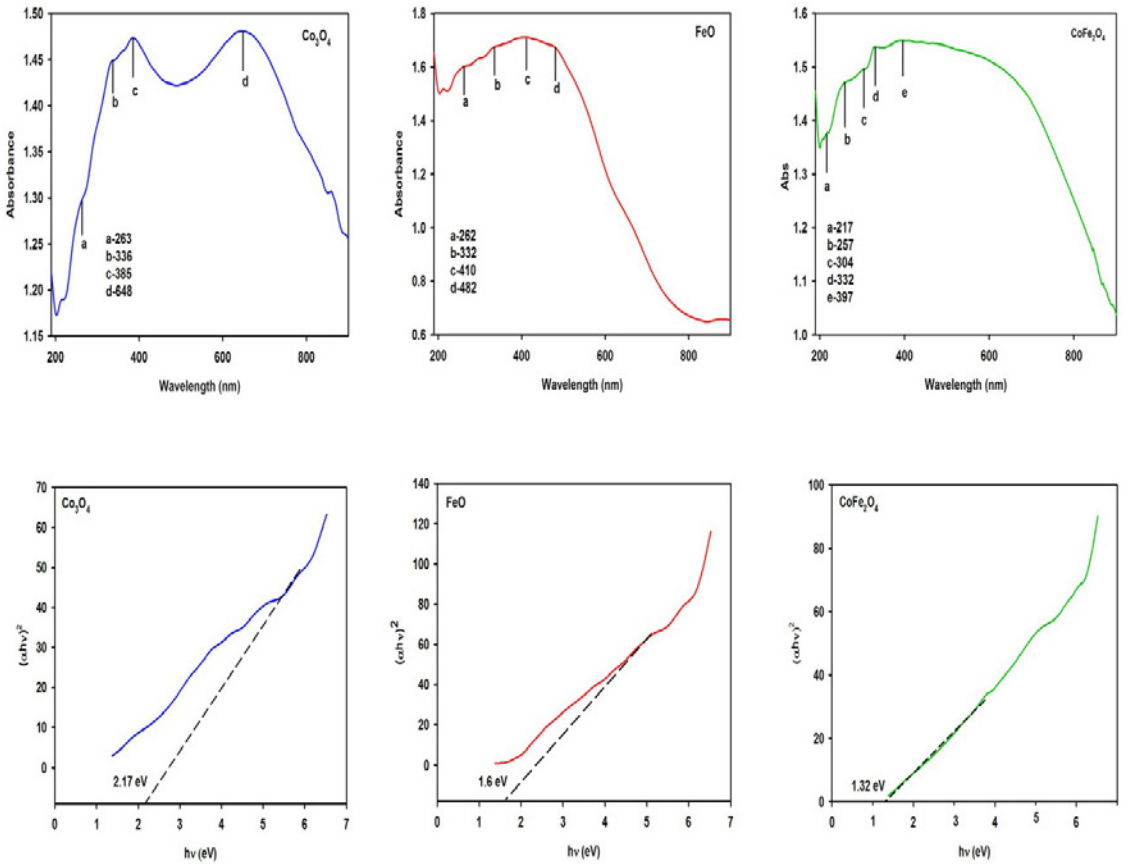

Fig. 6.UV-Vis diffuse reflectance spectra and tauk plots of cobalt oxide, iron oxide and cobalt ferrite nanoparticles prepared by wet chemical route after calcination

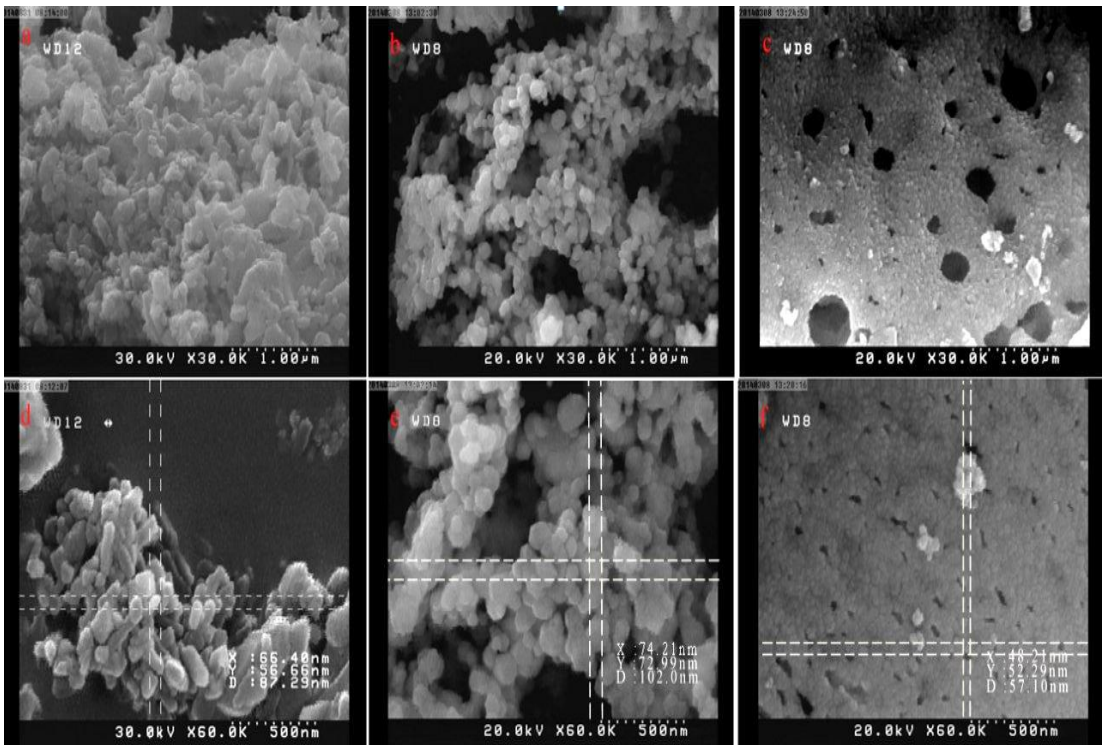

Fig. 7. FESEM pictures of FeO (A & D), Co_3O_4 (B & E), $CoFe_2O_4$(C & F) photocatalysts in 30000 and 60000 magnitude, respectively.

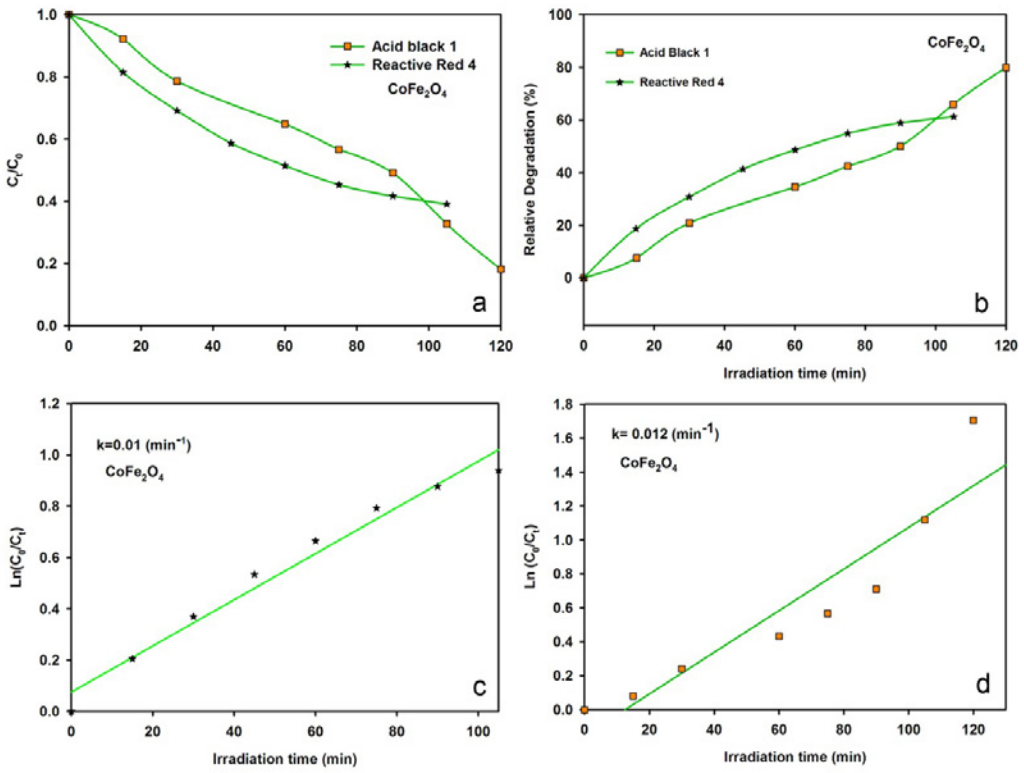

Fig. 8. a) Relative Concentration, b)Relative Degradation, c & d) kinetic parameters of Reactive Red 4 and Acid Black 1 degradation in presence of $CoFe_2O_4$ under UV light irradiation.

With respect to FESEM picture of FeO sample in (Fig. 7. a & d), it was found that FeO nanoparticles were grown in a cylindrical shape and the smallest dimension of their section was about 57 nm.

Photocatalytic degradation of azo dyes (AB1 & RR4) by $CoFe_2O_4$ nanoparticles

The photocatalytic degradation of RR4 and AB1 was performed under UV light irradiation by using CoFe2O4 nanoparticles coated on a glass slide as a photocatalyst. Fig. 8 shows the results of Reactive Red 4 and Acid Black 1 decomposition under UV light irradiation in the presence of $CoFe_2O_4$ coated on a glass slide.

The process of photocatalytic degradation of azo dyes over $CoFe_2O_4$ catalyst can be described as follows [42]. The first step involved adsorption of dye onto the surface of $CoFe_2O_4$ nanoparticles. Exposure of dye adsorbed $CoFe_2O_4$ nanoparticles to UV light led to the generation of electron-hole(e^--h^+)pairs in $CoFe_2O_4$ as indicated in the equation . The photo-generated electrons in the conduction band of $CoFe_2O_4$ interacted with the oxygen molecules adsorbed on $CoFe_2O_4$ to form superoxide anion radicals ($\cdot O_2^-$)(Eq. b). The holes generated in the valence band of $CoFe_2O_4$ reacted with surface hydroxyl groups to produce highly reactive hydroxyl radicals (Eq. c). These photo-generated holes could lead to dissociation of water molecules in the aqueous solution, producing radicals (Eq. d). The highly reactive hydroxyl radicals ($\cdot OH$) and superoxide radicals ($\cdot O_2^-$) could react with an azo dye adsorbed on $CoFe_2O_4$ nanoparticles and lead to its degradation as represent in (Eq. e and f).

$$CoFe_2O_4 + h\upsilon \rightarrow e^- (CB) + h^+(VB) \quad (a)$$

$$O_2 + e^- \rightarrow \cdot O^-_2 \quad (b)$$

$$h^+ + OH^- \rightarrow \cdot OH \quad (c)$$

$$h^+ + H_2O \rightarrow H^+ + \cdot OH^- \quad (d)$$

$$\cdot OH^- + \text{azo dye} \rightarrow \text{Degradation products} \quad (e)$$

$$\cdot O_2^- + \text{azo dye} \rightarrow \text{Degradation products} \quad (f)$$

The maximum absorbance of Reactive Red 4 decreased with increasing UV irradiation time until 105 min in presence of $CoFe_2O_4$ nanoparticles. $CoFe_2O_4$ photocatalyst decomposed Reactive Red 4 about 61% (Fig. 8.b). The slope of azo dyes in the curve of Relative concentration vs irradiation time was not constant therefore kinetic rate order could not be of zero order (Fig. 8.a). So the photocatalytic degradation kinetics of azo dyes was appraised with the first and second order equations given in (Eq.2, 3) and the corresponding plots were drawn, as shown in Fig. 8(c & d), the photocatalytic degradation kinetics of RR4 was first order and calculated rate constant was about 0.01(min^{-1}). Acid Black 1 was degraded by using photocatalyst under UV light in 120 min about %80 (Fig. 8. b). Degradation of Acid Black 1 by $CoFe_2O_4$ nanoparticles composite coated on glass followed first order rate kinetic and the rate constant was obtained around 0.012(min^{-1}) (Fig. 8. d). In this research, we made a comparison between the RR4 and AB1 degradations. It is noticeable that due attention to relative degradation graphs in (Fig. 8.b) the photocatalytic performance of $CoFe_2O_4$ in RR4 degradation was better than AB1 till 90 min. It was obviously found that $CoFe_2O_4$ performance in degradation of AB1 was more efficient than RR4 and the rate constant for AB1 was greater.

Photocatalytic degradation of azo dyes (AB1 & RR4) by Co_3O_4 nanoparticles

The photocatalytic activty of Co_3O_4 was also investigated through RR4 and AB1 degradation under UV light irradiation (Fig. 9). For both azo dyes the photocatalyst till 90 min had efficiency in dye degradation. The maximum absorbance of Reactive Red 4 and Acid Black 1 decreased with increasing UV irradiation time. The photocatalytic degradation of azo dyes over Co_3O_4 nanoparticles had the same procedure mentioned for $CoFe_2O_4$ at section (3.5). The Co_3O_4 nanoparticles degraded RR4 about 28% but 63% of AB1 was degraded (Fig .9.b). Degradation of RR4 using Co_3O_4 nanoparticles followed second order rate kinetic with rate constant equaled to 0.0004 ($ppm^{-1}.min^{-1}$) while the AB1 degradation followed first-order kinetic rate and rate constant was equal to 0.11(min^{-1}) (Fig. 9.c, d).

Fig 9. a) Relative Concentration, b)Relative Degradation, c & d) kinetic parameters of Reactive Red 4 and Acid Black 1 degradation in presence of Co_3O_4 under UV light irradiation.

Photocatalytic degradation of azo dyes (AB1 & RR4) by FeO nanoparticles

The photocatalytic performance of FeO nanoparticles was investigated for degradation of RR4 and AB1 under UV light irradiation. The relative concentration, relative degradation, and kinetic parameters are summarized in Fig. 10.

The degradation of RR4 under UV light irradiation in presence of FeO photocatalyst continued until 120 min and finally, 65% of RR4

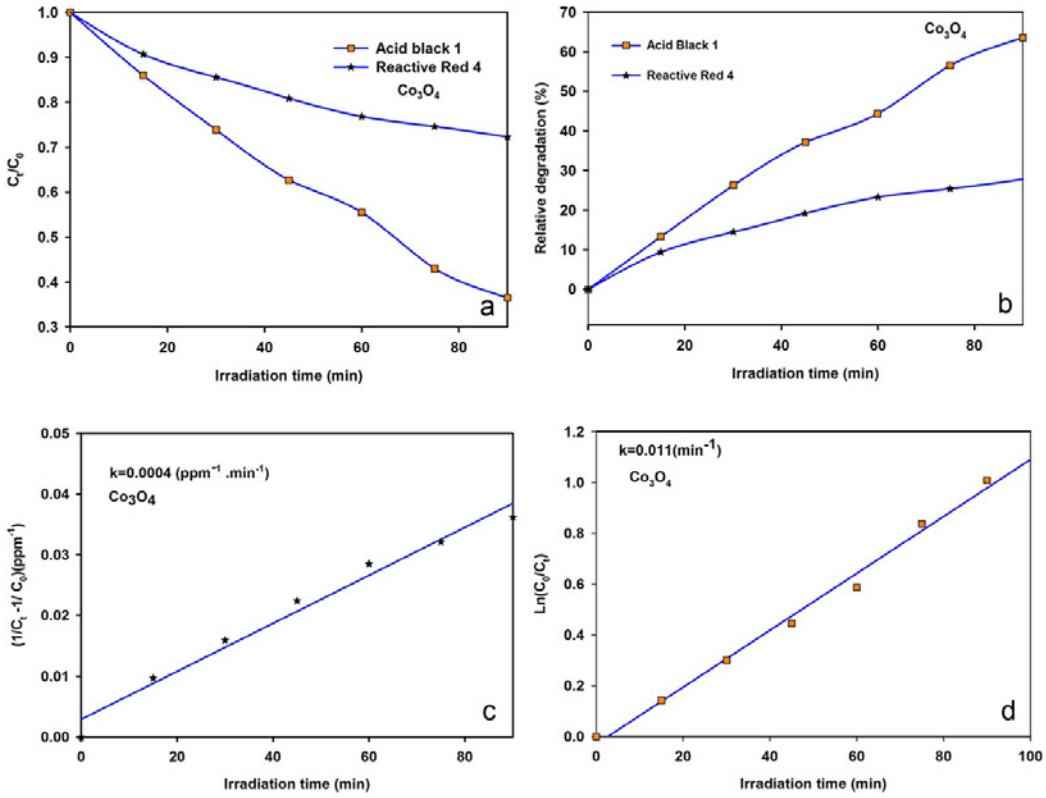

Fig. 9. a) Relative Concentration, b)Relative Degradation, c & d) kinetic parameters of Reactive Red 4 and Acid Black 1 degradation in presence of Co_3O_4 under UV light irradiation.

was degraded. The RR4 degradation by using FeO nanoparticles coated on a glass slide as photocatalyst had second order rate kinetic and rate constant was equal to 0.001ppm^{-1}.min^{-1}. The photocatalytic behavior of FeO nanoparticles coated on a glass slide in the degradation of AB1 was greatly different. UV-Vis absorbance spectra of AB1 showed a steady and slow degradation rate until 45 min UV irradiation but after 45 to 60 min the speed of degradation increased severely. Probably the reason for high-speed degradation was related to oxidation of iron from Fe^{2+} to Fe^{3+} and contribution of two iron species may have led to prompt of degradation. Another possible reason for the increase in speed was a photo-Fenton phenomenon. It seemed that during t=45-60 min the photocatalytic process and photo-Fenton phenomena had synergistic effects on degradation of dye. In the Fenton process, hydroxyl radicals are produced in the presence of an iron catalyst with degradation of hydrogen peroxide, according to the following Equations [i-g].

$$\cdot OH + \cdot OH \rightarrow H_2O_2^- \quad (i)$$

$$Fe^{2+} + H_2O_2 \rightarrow Fe^{3+} + \cdot OH + HO^- \quad (g)$$

Hydrogen peroxide is produced from a combination of hydroxyl groups. As seen, in this reaction, Fe^{+3} is produced which has low ability to catalyze hydroxyl radical. After UV ray irradiation in this reaction, Fe^{+3} is reduced to Fe^{+2}, therefore, the production of hydroxyl radicals is accelerated. This process is called as to Photo-Fenton Process:

$$Fe^{3+} + H_2O + h\nu \rightarrow Fe^{2+} + HO\cdot + H^+ \quad (h)$$

This reaction takes place after reaction (g) and continues with photo radiation. The efficiency of the Fenton reaction can be enhanced by using UV/vis irradiation. The main advantage of UV/vis irradiation is that Fe^{2+}species can be regenerated more quickly than the standard Fenton process, giving one more hydroxyl radical ready for the organic pollutants degradation (Fig. 11).

Relative concentration and degradation graphs of AB1 in a period of 45-60 mins show the rapid change that confirmed our probable suggestions (Fig. 10. a, b). According to the Fig. 12 the color

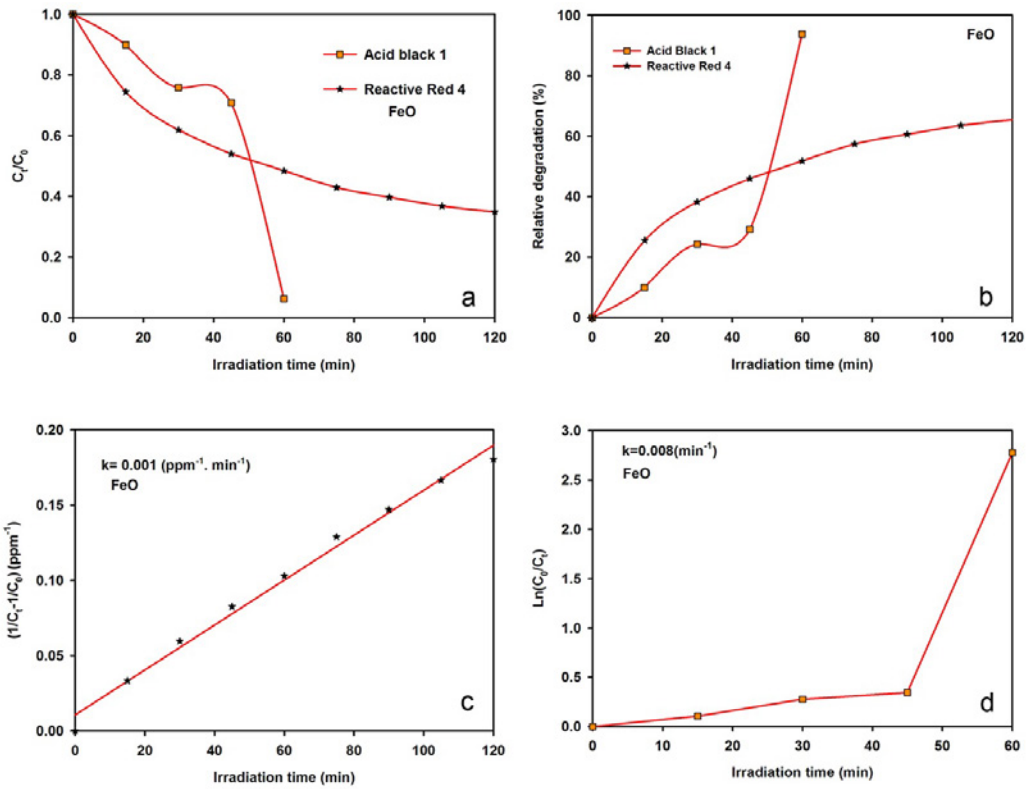

Fig.10. a) Relative Concentration, b)Relative Degradation, c& d) kinetic parameters of Reactive Red 4 and Acid Black 1 degradation in presence of FeO under UV light irradiation.

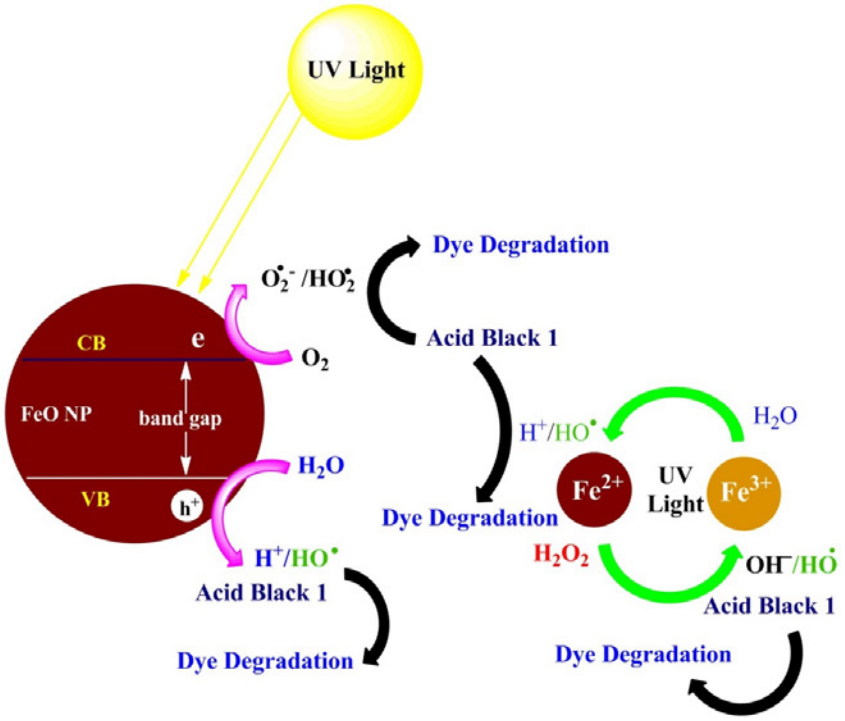

Fig.11. Proposed mechanism for AB1 degradation by photo-Fenton process and photocatalytic degradation over FeO nanoparticles under UV irradiation.

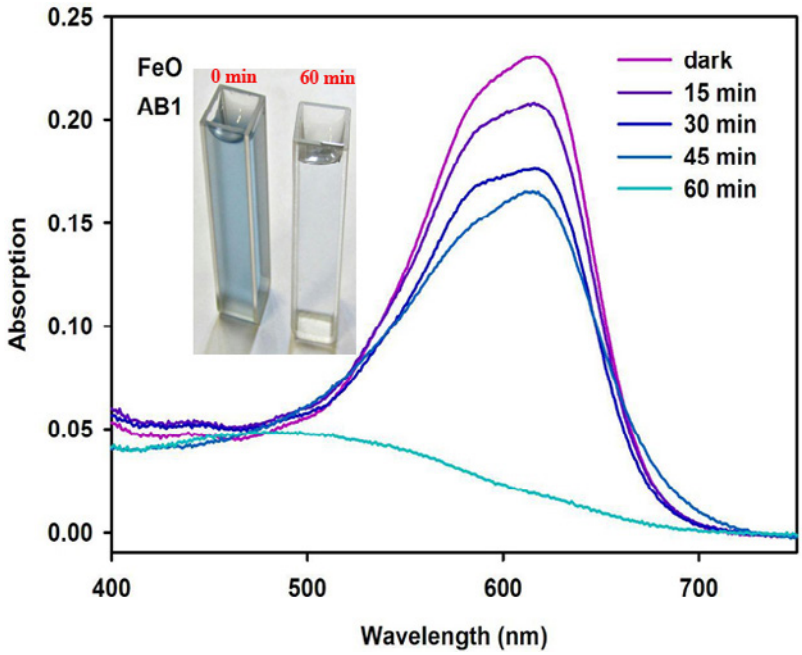

Fig.12. UV-Vis absorption spectra of Acid Black 1 degradation over FeO nanoparticles and picture of dye solution after 0 and 60 min UV irradiation.

Table. 1 .degradation condition (irradiation time (min) , relative degradation (%) , kinetic order and rate constant) of AB1 and RR4 over photocatalysts.

nano powder	Azo Dye	Relative degradation (%)	Irradiation time	Kinetic order	Rate Constant
$CoFe_2O_4$	AB1	80	120	1	0.012(min^{-1})
	RR4	61	105	1	0.01(min^{-1})
FeO	AB1	94	60	1	0.008(min^{-1})
	RR4	65	120	2	0.001($ppm^{-1}.min^{-1}$)
Co_3O_4	AB1	63	90	1	0.011(min^{-1})
	RR4	28	90	2	0.0004($ppm^{-1}.min^{-1}$)

of Acid Black 1 in 60 min UV irradiation over FeO nanoparticles converted to white, that confirmed the photo-Fenton process.

Degradation of AB1 obeyed first-order kinetic (0-45 min). The rate constant of the first period (0-45min) was calculated 0.008 min^{-1}.

Comparison of the photocatalytic degradation of AB1 and RR4 by $CoFe_2O_4$, Co_3O_4, and FeO

In degradation of AB1, FeO nanoparticles coated on glass had better performance in comparison with $CoFe_2O_4$ and Co_3O_4 nanoparticles. The relative degradation percent of AB1 decreased in the order of FeO>$CoFe_2O_4$>Co_3O_4. Degradation of AB1 by above-mentioned catalysts followed first order rate kinetics. The degradation rate of AB1 by photocatalysts decreased in the order of FeO > Co_3O_4> $CoFe_2O_4$. For degradation of RR4, FeO nanoparticles showed photocatalytic activity in a longer time than $CoFe_2O_4$ and Co_3O_4 and relative degradation percent decreased in the order of FeO>$CoFe_2O_4$>Co_3O_4. Degradation of RR4 by $CoFe_2O_4$ followed first order rate kinetic but the degradation of RR4 by FeO and Co_3O_4 followed second order rate kinetics. The rapidity of RR4 degradation by the aforementioned catalysts decreased in the order of $CoFe_2O_4$ > FeO >Co_3O_4. In the degradation of RR4, FeO had relatively better performance in comparison with CO_3O_4 and $CoFe_2O_4$. Table 1 summarizes degradation condition of azo dyes (AB1 & RR4) over photocatalysts ($CoFe_2O_4$, Co_3O_4, and FeO). Two main factors to determine photocatalytic performance are the band gap of photocatalyst and surface area (related to the particle size). For FeO, the further photo-Fenton process helps to degradation of azo dyes.

CONCLUSION

The $CoFe_2O_4$ composite and individual iron and cobalt oxide photocatalysts were synthesized by a wet chemical method that FTIR and XRD analysis results confirmed the formation of $CoFe_2O_4$, FeO and Co_3O_4. The morphological and optical properties of the photocatalysts were characterized by field emission scanning electron microscopy (FESEM) and diffuse reflectance spectroscopy (DRS), respectively. The photocatalysts nano-particles were coated on the glass by Doctor Blade method. Among the catalysts prepared, the FeO photocatalyst exhibited higher photocatalytic activity than Co_3O_4 and $CoFe_2O_4$ in the photocatalytic degradation of azo dyes such as RR4 and AB1 in water, which was due to the high specific surface area and photo-Fenton phenomena. The reaction in the degradation of AB1 by FeO was a photo-Fenton phenomena-like reaction. The degradation efficiency depended on free radical generation rate from Fe^{+2} and Fe^{+3}.

ACKNOWLEDGMENTS

The authors wish to thank the University of Isfahan for financial support of this work.

CONFLICT OF INTEREST

The authors declare that there are no conflicts of interest regarding the publication of this manuscript.

REFERENCES

1. da Silva Leite L, de Souza Maselli B, de Aragão Umbuzeiro G, Pupo Nogueira RF. Monitoring ecotoxicity of disperse red 1 dye during photo-Fenton degradation. Chemosphere. 2016;148:511-7.
2. de Jong L, Pech N, de Aragão Umbuzeiro G, Moreau X. Multi-scale biomarker evaluation of the toxicity of a commercial azo dye (Disperse Red 1) in an animal model, the freshwater cnidarian Hydra attenuata. Water Research. 2016;96:62-73.
3. Wu J, Wang J, Li H, Du Y, Huang K, Liu B. Designed synthesis of hematite-based nanosorbents for dye removal. Journal of Materials Chemistry A. 2013;1(34):9837.
4. Samiee S, Goharshadi EK. Graphene nanosheets as efficient adsorbent for an azo dye removal: kinetic and thermodynamic studies. Journal of Nanoparticle Research. 2014;16(8).
5. Lu Y-S, Bastakoti BP, Pramanik M, Malgras V, Yamauchi Y, Kuo S-W. Direct Assembly of Mesoporous Silica Functionalized with Polypeptides for Efficient Dye Adsorption. Chemistry - A European Journal. 2015;22(3):1159-64.
6. Ahmad R, Ahmad Z, Khan AU, Mastoi NR, Aslam M, Kim J. Photocatalytic systems as an advanced environmental remediation: Recent developments, limitations and new avenues for applications. Journal of Environmental Chemical Engineering. 2016;4(4):4143-64.
7. Sajjadi SH, Goharshadi EK. Highly monodispersed hematite cubes for removal of ionic dyes. Journal of Environmental Chemical Engineering. 2017;5(1):1096-106.
8. Li Z, Sheng J, Wang Y, Xu Y. Enhanced photocatalytic activity and stability of alumina supported hematite for azo-dye degradation in aerated aqueous suspension. Journal of Hazardous Materials. 2013;254-255:18-25.
9. Barreto-Rodrigues M, Silveira J, Zazo JA, Rodriguez JJ. Synthesis, characterization and application of nanoscale zero-valent iron in the degradation of the azo dye Disperse Red 1. Journal of Environmental Chemical Engineering. 2017;5(1):628-34.
10. Sun H, Cao L, Lu L. Magnetite/reduced graphene oxide nanocomposites: One step solvothermal synthesis and use as a novel platform for removal of dye pollutants. Nano Research. 2011;4(6):550-62.
11. Liang X, Zhong Y, He H, Yuan P, Zhu J, Zhu S, et al. The application of chromium substituted magnetite as heterogeneous Fenton catalyst for the degradation of aqueous cationic and anionic dyes. Chemical Engineering Journal. 2012;191:177-84.
12. Do TM, Byun JY, Kim SH. An electro-Fenton system using magnetite coated metallic foams as cathode for dye degradation. Catalysis Today. 2017;295:48-55.
13. Hagelin-Weaver HAE, Hoflund GB, Minahan DM, Salaita GN. Electron energy loss spectroscopic investigation of Co metal, CoO, and Co3O4 before and after Ar+ bombardment. Applied Surface Science. 2004;235(4):420-48.
14. Barrera E, González I, Viveros T. A new cobalt oxide electrodeposit bath for solar absorbers. Solar Energy Materials and Solar Cells. 1998;51(1):69-82.
15. Patil PS, Kadam LD, Lokhande CD, Thin Solid Films 272, 29-32 (1996).
16. Long M, Cai W, Cai J, Zhou B, Chai X, Wu Y. Efficient Photocatalytic Degradation of Phenol over Co3O4/BiVO4Composite under Visible Light Irradiation. The Journal of Physical Chemistry B. 2006;110(41):20211-6.
17. Shao H, Zhao X, Wang Y, Mao R, Wang Y, Qiao M, et al. Synergetic activation of peroxymonosulfate by Co3O4 modified g-C3N4 for enhanced degradation of diclofenac sodium under visible light irradiation. Applied Catalysis B: Environmental. 2017;218:810-8.
18. Al Nafiey A, Addad A, Sieber B, Chastanet G, Barras A, Szunerits S, et al. Reduced graphene oxide decorated with Co 3 O 4 nanoparticles (rGO-Co 3 O 4) nanocomposite: A reusable catalyst for highly efficient reduction of 4-nitrophenol, and Cr(VI) and dye removal from aqueous solutions. Chemical Engineering Journal. 2017;322:375-84.
19. Nassar MY, Mohamed TY, Ahmed IS, Mohamed NM, Khatab M. Hydrothermally Synthesized Co3O4, α-Fe2O3, and CoFe2O4 Nanostructures: Efficient Nano-adsorbents for the Removal of Orange G Textile Dye from Aqueous Media. Journal of Inorganic and Organometallic Polymers and Materials. 2017;27(5):1526-37.
20. Thomas B, Alexander LK. Enhanced synergetic effect of Cr(VI) ion removal and anionic dye degradation with superparamagnetic cobalt ferrite meso–macroporous nanospheres. Applied Nanoscience. 2018;8(1-2):125-35.
21. Hassani A, Eghbali P, Ekicibil A, Metin Ö. Monodisperse

cobalt ferrite nanoparticles assembled on mesoporous graphitic carbon nitride (CoFe2O4/mpg-C3N4): A magnetically recoverable nanocomposite for the photocatalytic degradation of organic dyes. Journal of Magnetism and Magnetic Materials. 2018;456:400-12.
22. Habibi MH, Parhizkar HJ. FTIR and UV–vis diffuse reflectance spectroscopy studies of the wet chemical (WC) route synthesized nano-structure CoFe2O4 from CoCl2 and FeCl3. Spectrochimica Acta Part A: Molecular and Biomolecular Spectroscopy. 2014;127:102-6.
23. Li C-J, Wang J-N, Wang B, Gong JR, Lin Z. A novel magnetically separable TiO2/CoFe2O4 nanofiber with high photocatalytic activity under UV–vis light. Materials Research Bulletin. 2012;47(2):333-7.
24. Yang X, Cao C, Erickson L, Hohn K, Maghirang R, Klabunde K. Photo-catalytic degradation of Rhodamine B on C-, S-, N-, and Fe-doped TiO2 under visible-light irradiation. Applied Catalysis B: Environmental. 2009;91(3-4):657-62.
25. Wang Q, Xu S, Shen F. Preparation and characterization of TiO2 photocatalysts co-doped with iron (III) and lanthanum for the degradation of organic pollutants. Applied Surface Science. 2011;257(17):7671-7.
26. Mathews NR, Jacome MAC, Morales ER, Antonio JAT. Structural and spectroscopic study of the Fe doped TiO2 thin films for applications in photocatalysis. physica status solidi (c). 2009;6(S1):S219-S23.
27. Khandekar MS, Kambale RC, Patil JY, Kolekar YD, Suryavanshi SS. Effect of calcination temperature on the structural and electrical properties of cobalt ferrite synthesized by combustion method. Journal of Alloys and Compounds. 2011;509(5):1861-5.
28. Boobalan T, Suriyanarayanan N, Pavithradevi S. Structural, magnetic and dielectric properties of nanocrystalline cobalt ferrite by wet hydroxyl chemical route. Materials Science in Semiconductor Processing. 2013;16(6):1695-700.
29. Rana S, Philip J, Raj B. Micelle based synthesis of cobalt ferrite nanoparticles and its characterization using Fourier Transform Infrared Transmission Spectrometry and Thermogravimetry. Materials Chemistry and Physics. 2010;124(1):264-9.
30. Cannas C, Ardu A, Peddis D, Sangregorio C, Piccaluga G, Musinu A. Surfactant-assisted route to fabricate CoFe2O4 individual nanoparticles and spherical assemblies. Journal of Colloid and Interface Science. 2010;343(2):415-22.
31. Salavati-Niasari M, Khansari A, Davar F. Synthesis and characterization of cobalt oxide nanoparticles by thermal treatment process. Inorganica Chimica Acta. 2009;362(14):4937-42.
32. Barakat NAM, Khil MS, Sheikh FA, Kim HY. Synthesis and Optical Properties of Two Cobalt Oxides (CoO and Co3O4) Nanofibers Produced by Electrospinning Process. The Journal of Physical Chemistry C. 2008;112(32):12225-33.
33. Tang C-W, Wang C-B, Chien S-H. Characterization of cobalt oxides studied by FT-IR, Raman, TPR and TG-MS. Thermochimica Acta. 2008;473(1-2):68-73.
34. Lin, H. K., Wang, C. B., Chiu, H. C., & Chien, S. H. (2003). In situ FTIR study of cobalt oxides for the oxidation of carbon monoxide. Catalysis letters, 86(1-3), 63-68.
35. Li C-J, Wang J-N, Wang B, Gong JR, Lin Z. A novel magnetically separable TiO2/CoFe2O4 nanofiber with high photocatalytic activity under UV–vis light. Materials Research Bulletin. 2012;47(2):333-7.
36. Wang JA, Limas-Ballesteros R, López T, Moreno A, Gómez R, Novaro O, et al. Quantitative Determination of Titanium Lattice Defects and Solid-State Reaction Mechanism in Iron-Doped TiO2Photocatalysts. The Journal of Physical Chemistry B. 2001;105(40):9692-8.
37. NavõÂoa JA, Testab JJ, Djedjeianb P, PadroÂnb JR, RodrõÂguezb D, Litterb MI,Appl. Catal., A 178, 203 (1999).
38. Shoeb M, Singh BR, Khan JA, Khan W, Singh BN, Singh HB, et al. ROS-dependent anticandidal activity of zinc oxide nanoparticles synthesized by using egg albumen as a biotemplate. Advances in Natural Sciences: Nanoscience and Nanotechnology. 2013;4(3):035015.
39. Nouroozi F, Farzaneh F. Synthesis and characterization of brush-like ZnO nanorods using albumen as biotemplate. Journal of the Brazilian Chemical Society. 2011;22(3):484-8.
40. Habibi MH, Parhizkar J. Cobalt ferrite nano-composite coated on glass by Doctor Blade method for photo-catalytic degradation of an azo textile dye Reactive Red 4: XRD, FESEM and DRS investigations. Spectrochimica Acta Part A: Molecular and Biomolecular Spectroscopy. 2015;150:879-85.
41. Choi HW, Kim EJ, Hahn SH. Photocatalytic activity of Au-buffered WO3 thin films prepared by RF magnetron sputtering. Chemical Engineering Journal. 2010;161(1-2):285-8.
42. Konstantinou IK, Albanis TA. TiO2-assisted photocatalytic degradation of azo dyes in aqueous solution: kinetic and mechanistic investigations. Applied Catalysis B: Environmental. 2004;49(1):1-14.